# Interacting valley Chern insulator and its topological imprint on moiré superconductors

Xiao-Chuan Wu,[1] Yichen Xu,[1] Chao-Ming Jian,[2] and Cenke Xu [1]

[1]*Department of Physics, University of California, Santa Barbara, California 93106, USA*
[2]*Kavli Institute of Theoretical Physics, Santa Barbara, California 93106, USA*

One salient feature of systems with moiré superlattice is that the Chern number of "minibands" originating from each valley of the original graphene Brillouin zone becomes a well-defined quantized number because the miniband from each valley can be isolated from the rest of the spectrum due to the moiré potential. Then a moiré system with a well-defined valley Chern number can become a nonchiral topological insulator with $U(1) \times Z_3$ symmetry and a $\mathbb{Z}$ classification at the free fermion level. Here we demonstrate that the strongly interacting nature of the moiré system reduces the classification of the valley Chern insulator from $\mathbb{Z}$ to $\mathbb{Z}_3$, and it is topologically equivalent to a bosonic symmetry-protected topological state made of local boson operators. We also demonstrate that even if the system becomes a superconductor when doped away from the valley Chern insulator, the valley Chern insulator still leaves a topological imprint as the localized Majorana fermion zero mode in certain geometric configuration.

## I. INTRODUCTION

Systems with moiré superlattices not only have demonstrated amazing correlated physics such as correlated insulator at fractional filling and also superconductivity [1–11], due to the narrow width of the moiré minibands [9–15], but recent theoretical and experimental studies have shown that under certain conditions some of the moiré systems can also have novel topological features. The reason is that within the mini Brillouin zone, the miniband that originates from each valley of the original graphene Brillouin zone can be isolated from the rest of the spectrum, which makes the Chern number of a miniband from each valley a well-defined quantized Chern number. Indeed, many theoretical works have predicted that the Chern number of minibands from each valley can take different integer values in various moiré systems, depending on the displacement field and also the twisted angle [16–19]. Recently, quantized [20] (or unquantized [6]) Hall conductivity has been observed at doping with one or three electrons or holes per moiré unit cell away from charge neutrality in some moiré systems, whose most natural explanation is that under the experimental conditions the moiré system forms a fully spin and valley polarized state [20–22], hence a miniband with a net Chern number is completely filled. Although superconductivity has not been observed near the insulating states with nonzero Hall conductivity, this topological physics is certainly interesting in its own right.

Here we study the nonchiral valley Chern insulator (VCI), namely, the valley space is not polarized, while instead we assume the spin space is fully polarized. These assumptions may be relevant to the twisted double bilayer graphene (TDBG) at half-filling (two extra electrons per moiré unit cell) away from charge neutrality [7,9–11], for the following reasons:

(i) Calculations with various methods have demonstrated that in TDBG the minibands from each valley [16,18,19] could have a nonzero quantized Chern number depending on the displacement field and also twisted angle. Symmetry of the system guarantees that the degenerate minibands from the two valleys must have opposite Chern numbers. If the partially filled miniband has a zero valley Chern number (with certain displacement field), then the formalism developed in Refs. [23–26] becomes applicable. In this work we assume a nonzero valley Chern number of the minibands.

(ii) The charge gap of the insulator at half-filling increases with in-plane magnetic field [7,9–11], whose main effect is most likely a Zeeman coupling with spin. This phenomenon suggests that the insulator at half-filling observed in this system has a fully polarized ferromagnetic order.

(iii) Superconductivity is observed near half-filling, which suggests that the valley space is likely unpolarized, because otherwise electron states with momentum $\vec{k}$ and $-\vec{k}$ would be nondegenerate, which makes pairing with total zero momentum difficult. Even within each valley, the $C_3$ symmetry of the Fermi surface still does not guarantee degeneracy of states with momentum $\vec{q}$ and $-\vec{q}$, where $\vec{q}$ is the momentum away from each valley.

These observations plus simple counting suggest that at half-filling (with two extra electrons per moiré unit cell away from the charge neutrality), the insulator observed in TDBG could be a spin-polarized "band insulator" where spin-down electrons fill both minibands whose total valley Chern number is zero for a relatively weak displacement field [19], while spin-up electrons only fill the valence miniband with nonzero Chern number. Then the system becomes a spin-polarized nonchiral topological insulator, or a valley Chern insulator (VCI). The symmetry of this VCI is $U(1) \times Z_3$, where the $U(1)$ corresponds to the charge conservation, and $Z_3$ is the conservation of the "valley quantum number" (valley momentum of the original graphene Brillouin zone is conserved mod 3).

## II. INTERACTING VALLEY CHERN INSULATOR

At the free fermion level, the Hamiltonian of the 1$d$ edge state of the VCI with valley Chern number $C = 1$ is ($C = 1$ means the minibands from the right and left valleys have Chern number $\pm 1$ respectively)

$$H = \int dx \, \psi^\dagger (-i\tau^z \partial_x)\psi, \qquad (1)$$

where $\tau^z = \pm 1$ represents the edge modes from the right and left valleys. The $Z_3$ symmetry acts on the boundary electron operator as $Z_3 : \psi \to [\exp(i\frac{2\pi}{3}\tau^z)]\psi$. The $Z_3$ symmetry guarantees that no fermion bilinear mass term can be added to the boundary Hamiltonian. Also, for arbitrary copies of the VCI, or for states with arbitrary valley Chern number, fermion bilinear mass operators are always forbidden by the $Z_3$ symmetry. Hence the classification of VCI in the noninteracting limit is $\mathbb{Z}$.

The moiré systems are intrinsically strongly interacting systems, thus we need to understand the effects of interaction on the VCI. In the last decade, examples have been found where interaction can indeed change the classification of topological insulators [27–35], though usually interaction would reduce the classification of a topological insulator from $\mathbb{Z}$ to $\mathbb{Z}_8$, or $\mathbb{Z}_{16}$. In the following we will demonstrate that an interacting VCI actually has a $\mathbb{Z}_3$ classification.

The VCI can be naturally embedded into a nonchiral topological insulator (TI) with U(1)$_c \times$ U(1)$_s$ symmetry, which is analogous to the quantum spin Hall insulator, and the valley space can be viewed as a pseudospin space, with pseudospin $\tau^z = \pm 1$ labeling the right and left valley spaces. We will start with the TI with U(1)$_c \times$ U(1)$_s$ symmetry.[1] There are only two elementary fermions with charge $(1,1)$ and $(1, -1)$ under the U(1)$_c \times$ U(1)$_s$ symmetry, and for the simplest case they form Chern insulators with Chern number $\pm 1$ respectively. Such a TI has a topological response:

$$\mathcal{L}^r = \frac{2i}{2\pi} A_c \wedge dA_s, \qquad (2)$$

where $A_c$ and $A_s$ are background gauge fields that couple to the U(1)$_c$ and U(1)$_s$ symmetries, and an electron carries charge $-1$ under $A_c$ and charge $\pm 1$ under $A_s$.

In the following, we will consider the the consequence of breaking U(1)$_s$ to its discrete subgroups. When we break U(1)$_c \times$ U(1)$_s$ symmetry down to U(1)$_c \times \mathbb{Z}_n$, the fermions transform under $Z_n$ as

$$Z_n : \psi_1 \to e^{2\pi i/n}\psi_1, \quad \psi_2 \to e^{-2\pi i/n}\psi_2. \qquad (3)$$

To describe the nonchiral TI, we can use the $K$-matrix formalism [36]. The system can be described by the following Chern-Simons theory:

$$\mathcal{L} = \frac{i}{4\pi} \sum_{A,B=1,2} K^{AB} a^A \wedge da^B, \quad K = \begin{pmatrix} 1 & 0 \\ 0 & -1 \end{pmatrix}, \qquad (4)$$

where $a^A$ with $A = 1, 2$ are two dynamical U(1) gauge fields. The edge state of this TI is described by the Luttinger liquid theory with two chiral boson fields $\phi_1$, $\phi_2$ and the same $K$-matrix above [37,38]:

$$\mathcal{L}_{\text{edge}} = \sum_{A,B=1,2} \frac{K^{AB}}{4\pi} \partial_x \phi_A \partial_t \phi_B - \frac{V^{AB}}{4\pi} \partial_x \phi_A \partial_x \phi_B, \qquad (5)$$

where $V$ is a $2 \times 2$ positive-definite velocity matrix. In this theory, the boson fields satisfy the equal time commutation relation $[\phi_A(x), \partial_y \phi_B(y)] = 2\pi i (K^{-1})^{AB} \delta(x - y)$. Under the U(1)$_c \times Z_n$ symmetry, the chiral boson fields $\phi_{1,2}$ transform as

$$\text{U(1)}_c : \phi_{1,2} \to \phi_{1,2} + \alpha, \quad Z_n : \phi_{1,2} \to \phi_{1,2} \pm \frac{2\pi}{n}. \qquad (6)$$

Now we demonstrate that the nonchiral TI with U(1)$_c \times Z_n$ symmetry at most has a $\mathbb{Z}_n$ classification under local interaction, for odd integer $n$. The fact that $n$ copies of such TI together are topologically trivial can be seen from the edge theory of this system which consists of $n$ copies of Luttinger liquid theory, Eq. (5). Let us denote chiral boson fields in this $n$-copy Luttinger liquid theory as $\phi_{i,A}$ where $i = 1$ is the copy index and $A = 1, 2$ is the label for the chiral bosons within each copy. The boundary of $n$ copies of the TI can be gapped out by the following symmetric boundary interaction without ground-state degeneracy:

$$\mathcal{L}_{\text{edge}}^{(1)} = -g \cos\left(\sum_{i=1}^{n} (\phi_{i,1} - \phi_{i,2})\right)$$

$$- g' \sum_{i=1}^{n-1} \cos(\phi_{i,1} + \phi_{i,2} - \phi_{i+1,1} - \phi_{i+1,2}). \qquad (7)$$

These are local interacting terms between the electrons.

This edge theory $\mathcal{L}_{\text{edge}}^{(1)}$ can be analyzed systematically as follows: There are in total $n$ different terms in $\mathcal{L}_{\text{edge}}^{(1)}$, and we can represent each term in $\mathcal{L}_{\text{edge}}^{(1)}$ as $\cos(\Lambda_I \cdot \Phi)$. $\Lambda_I$ are $2n$ component vectors ($I = 1, \ldots, n$), and $\Phi = (\phi_{1,1}, \phi_{1,2}, \phi_{2,1}, \ldots)$. $\Lambda_I$ are a set of minimal linearly independent integer vectors, and they satisfy the condition [39,40]

$$\Lambda_I^t K^{-1} \Lambda_J = 0, \qquad (8)$$

for any $I, J = 1, \ldots, n$. Here $\mathbf{K}$ is the $2n \times 2n$ block-diagonal $K$ matrix for $n$ copies of the nonchiral TI with U(1)$_c \times Z_n$ symmetry. Equation (8) implies that the arguments in all the cosine terms in $\mathcal{L}_{\text{edge}}^{(1)}$ commute with each other, and hence all terms in $\mathcal{L}_{\text{edge}}^{(1)}$ can be minimized simultaneously.

The $2n$-component integer vector $\Lambda_I$ is a vector in a $2n$-dimensional cubic lattice with lattice constant 1. Linear combinations of $\Lambda_I$ span an $n$-dimensional hyperplane of this $2n$-dimensional cubic lattice. Linear combinations of $\Lambda_I$ span an $n$-dimensional hyperplane of this $2n$-dimensional cubic lattice. To be rigorous we also need to show that $\Lambda_I$ are the irreducible basis vectors of the lattice sites residing on this $n$-dimensional hyperplane, hence the minimum of $\mathcal{L}_{\text{edge}}^{(1)}$ has no degeneracy. This has been verified for odd integer $n$, which leads to a fully gapped edge state. Similar reduction of classification was also discussed in a different context [41].

---

[1]More precisely the symmetry of this system is in fact $\frac{\text{U(1)}_c \times \text{U(1)}_s}{Z_2}$, which means that the $Z_2$ subgroup of U(1)$_c$ is identified with that of the U(1)$_s$, but we will ignore this subtlety.

The formalism above will lead to the same conclusion with other observations. For example, the response to the external gauge field Eq. (2) implies that for a $C = 3$ VCI, a $2\pi$ flux of the electromagnetic field would nucleate a trivial $Z_3$ charge according to Eq. (2). The fact that the VCI is generically trivial when $C = 3$ implies that this interacting VCI can be adiabatically deformed into a spatially direct product state under interaction without closing the gap in the bulk, and the deformation process preserves all the symmetries. This result is relevant to the TDBG with certain displacement field [18,19], and the valence/hole miniband of the heterostructure of trilayer graphene and hexagonal boron nitride [16,17]. In these cases calculations suggest that the valley Chern number is $C = 3$ in the noninteracting limit.

There is a three-body interaction (six-body term) in Eq. (1) that breaks the valley-U(1) symmetry [analog of the U(1)$_s$ in the quantum spin Hall insulator] to the physical $Z_3$ symmetry. This three-body interaction originates from a second-order effect of lattice-scale short-range interactions which allow large momentum transfer. Here we will give a rudimentary estimate of the strength of this effect. We consider a scattering process of three-particle wave packets from valley 1 to valley 2: $\{\vec{Q}, \vec{Q}, \vec{Q}\} \to \{-\vec{Q}, -\vec{Q}, -\vec{Q}\}$, where $\vec{Q}$ is the momentum of valley 1 in the original graphene Brillouin zone. Each wave packet has the size of the moiré unit cell $l^2$, where $l$ is the moiré lattice constant and $l \approx 1/[2\sin(\theta/2)]$ (we are viewing $l$ as the dimensionless ratio between the moire lattice spacing and the lattice constant of the original graphene). This process can come from a second-order effect of two combined processes: $\{\vec{Q}, \vec{Q}\} \to \{-\vec{Q}, \Gamma\}$, and $\{\vec{Q}, \Gamma\} \to \{-\vec{Q}, -\vec{Q}\}$, where $\Gamma$ corresponds to the state with momentum 0 in the graphene Brillouin zone. The strength of this scattering process is roughly $g \approx l^2 U^2 / (E_\Gamma) 1/l^6$, where $U$ is the total short-range interaction in each unit cell of the original lattice. For example, since we are mostly considering spinless fermions motivated from the fact that in TDBG the electron spins are fully polarized in a large region of the phase diagram, we only consider the nearest neighbor repulsions, which is about 5.5 eV according to Ref. [42]. There are six nearest neighbor pairs of sites (in total eight sites) within one unit cell of the double bilayer graphene, including both in-plane and vertical pairs. Hence we roughly estimate $U \approx 5.5 \times 6$ eV. $E_\Gamma$ is the energy of the electron at momentum 0, which is about 4.9 eV choosing the same parameter as in Fig. 3 of Ref. [43]. The first factor $l^2$ is from summing over all sites in the moiré unit cell, and the last factor $1/l^6$ is due to the fact that if the wave-function packet is normalized in each moiré unit cell, the amplitude of the wave function on each site will be $1/l$. Choosing $\theta = 1.33$ as in experiment Ref. [7,10], we eventually obtain $g \approx 0.65K$, which is not strong, but its effect is still observable experimentally. If further neighbor interaction in graphene is considered [42], this effect will be further enhanced.

## III. BOSONIC SYMMETRY-PROTECTED TOPOLOGICAL STATE

For odd integer $n$, a general connection between the nonchiral TI with U(1) × $Z_n$ symmetry and the bosonic symmetry-protected topological (bSPT) state [44,45] can be made. Since the interacting TI has a $\mathbb{Z}_n$ classification, one copy of the elementary TI is topologically equivalent to $n + 1$ (an even integer) copies of the TI; while according to Refs. [46–49], an even number of such TIs can be "glued" into a bSPT state with the same symmetry under interaction, where all the local fermion excitations at the boundary are gapped out by interaction, leaving only symmetry-protected gapless local bosonic excitations.

A variety of bSPT states and their edge states can be described by the Chern-Simons theory with the following $K$ matrix [50], whose boundary state is described by two chiral bosons $\varphi$ and $\theta$ with $K$ matrix:

$$K_{\text{bSPT}} = \begin{pmatrix} 0 & 1 \\ 1 & 0 \end{pmatrix}. \tag{9}$$

The chiral bosons transform under the symmetries as

$$\begin{aligned} \text{U(1)}_c &: \varphi \to \varphi + 2\alpha, \quad \theta \to \theta, \\ Z_n &: \varphi \to \varphi, \quad \theta \to \theta - 2\pi/n. \end{aligned}$$

Now, we consider a $(1 + 1)d$ interface between the bSPT and the nonchiral TI discussed previously which can be described by the four boson fields $\phi_{1,2}$, $\varphi$, and $\theta$. The symmetry-allowed interaction that can gap out this interface without degeneracy is

$$\mathcal{L}_{\text{edge}}^{(2)} \approx -u_1 \cos(\phi_1 + \phi_2 - \varphi) - u_2 \cos(\phi_1 - \phi_2 + 2\theta). \tag{10}$$

Again the arguments in the cosine terms commute with each other, hence all terms in $\mathcal{L}_{\text{edge}}^{(2)}$ can be minimized simultaneously, and the interface is gapped out without degeneracy through the same reasoning as in the last section. The existence of such a gapped interface between the bSPT and the fermionic TI guarantees the topological equivalence between the two sides of this interface.

The physical interpretation of the bosonic fields $\varphi$ and $\theta$ can be understood in terms of their quantum numbers. The local boson field $e^{i\varphi}$ can be identified with the bound state $\psi_1\psi_2$; the quantum number of the single boson operator $e^{i\theta}$ is equivalent to $(n + 1)/2$ copies of the particle-hole pair $\psi_1^\dagger \psi_2$ ($Z_n$ charge is defined mod $n$). We can see that *when and only when $n$ is an odd integer*, $e^{i\theta}$ can be viewed as a local boson field. Hence for odd integer $n$, a nonchiral TI with U(1) × $Z_n$ symmetry is equivalent to a bSPT constructed with local bosons. This result implies that under interaction any VCI in the moiré system can have fully gapped single-electron excitation, but meanwhile symmetry-protected gapless local boson excitations occur at its boundary. This was thought to be only possible for *even* copies of nonchiral TI such as the quantum spin Hall insulator with spin $S^z$ conservation [46–49].

In the spin-polarized moiré system there is one more natural symmetry, an effective time-reversal symmetry which is a product between the ordinary time reversal of electron and spin flipping. This time-reversal symmetry acts on the electron as

$$\mathcal{T} : \psi \to \tau^x \psi, \tag{11}$$

and it has $\mathcal{T}^2 = +1$. All our conclusions above including the classification of interacting VCI and its connection to bSPT still hold with this extra effective time reversal.
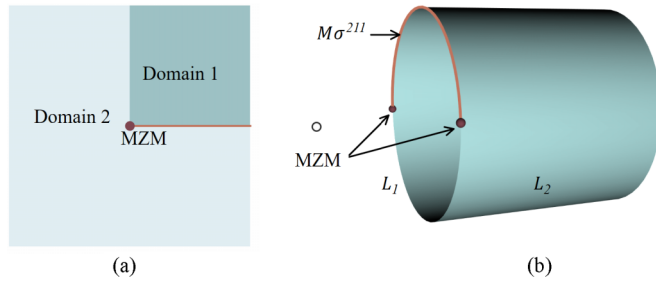
FIG. 1. (a) The proposed experimental geometry for detecting the Majorana zero mode (MZM). The entire system is the TDBG in its spin-polarized superconductor phase near half-filling away from charge neutrality [7,9,10]. Displacement field (out of plane) is adjusted such that the valley Chern numbers of the filled minibands differ by 1 between the two domains. The vertical domain wall preserves the valley quantum number, while the horizontal domain wall breaks the valley quantum number conservation. We propose that a MZM is located at the 0*d* junction between the two domain walls. (b) The geometry of our effective lattice model. The 1*d* domain walls in (a) are modeled by the open boundary of Eq. (12) defined on a cylinder with size $20 \times 20$. The horizontal domain wall in (a) is modeled by an intervalley scattering $M\sigma^{211}$ on half of the boundary.

## IV. TOPOLOGICAL IMPRINT OF VCI: MAJORANA ZERO MODE

A deconfined Majorana zero mode (MZM) is a non-Abelian anyon excitation [51–54]. MZM can be engineered in various designs [55–59], including the vortex core of the proximity superconductor at the boundary of a 3*d* topological insulator [60,61]. Later it was realized that the proximity superconductivity at the boundary of a 3*d* TI can be directly enforced if the bulk of the system forms a superconductor when doped with finite charge carrier density. Even if strictly speaking the bulk superconductor is topologically trivial, the MZM at the boundary vortex core can still survive [62]. Recently the topological nature of the band structure of the iron-pnictide and iron-chalcogenide materials was discussed [63–66], and MZM in the boundary vortex core was observed in iron-based superconductors [67,68].

Here we propose the possibility of a localized MZM at certain geometric defect of the moiré superconductor when the system is doped away from the VCI. Evidence of spin-polarized VCI, and spin-polarized superconductivity were observed in TDBG near half-filling away from the charge neutrality [7,9,10]. We consider the geometry of Fig. 1(a), where the displacement field of the two domains is tuned such that the valley Chern numbers of the filled valence miniband of the spin-up electron differ by $\Delta C = 1$ between the two domains (the spin-down electrons fill both minibands and have total zero valley Chern number). The vertical domain wall in Fig. 1(a) preserves the valley conservation of the original graphene sheet, while the horizontal domain wall breaks the valley conservation. Our conclusion is that at the 0*d* junction of the two domain walls, there can be a MZM which can be viewed as the imprint of the topological effect of the VCI, even if the system is already doped away from the VCI and forms a superconductor.
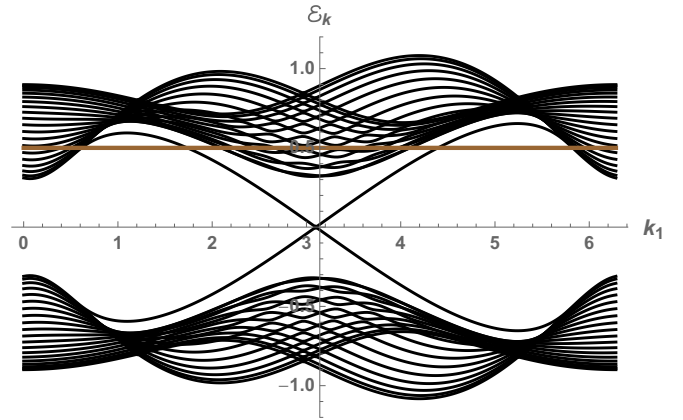


FIG. 2. The band structure of our effective lattice model for each valley with two open boundaries. As we can see there are two counterpropagating edge modes from the two boundaries. We have chosen $t_1 = 0.3$, $t_2 = 0.2$, and $m = 0.05$ in our effective model, Eq. (12). The horizontal line is the energy (chemical potential) $\mu = 0.5$.

We model the 1*d* domain wall of Fig. 1(a) as the open boundary of an effective model. The contribution from each valley is modeled by a Haldane model [69] for a Chern insulator defined on a honeycomb lattice:

$$H_v = t_1 \sum_{\langle i,j \rangle} c_i^\dagger c_j + \eta_v t_2 \sum_{\langle\langle i,j \rangle\rangle} i c_i^\dagger c_j + \text{H.c.}, \qquad (12)$$

where $\eta_v = \pm 1$ for the two different valleys, hence the minibands from the two valleys carry the opposite Chern number. We also turn on a small staggered potential energy $m\eta_v(-1)^j c_j^\dagger c_j$ between the two sublattices to break the symmetry of the system down to $C_3$ (same as the miniband at each valley of the moiré system), while keeping the nontrivial band topology. Please notice that the lattice of this effective model is not the original graphene sheet. The unit cell of this effective lattice coincides with the moiré unit cell. The band structure of this model with two open boundaries [Fig. 1(b)] is plotted in Fig. 2.

We turn on a nonzero chemical potential $\mu$, and also a uniform *s*-wave valley-singlet superconductor order parameter $\Delta$ in the entire system. The entire bulk Hamiltonian in the Majorana fermion basis reads

$$\mathcal{H}_k^{\text{BdG}} = d_1(\boldsymbol{k})\sigma^{201} + d_2(\boldsymbol{k})\sigma^{202} + d_3(\boldsymbol{k})\sigma^{033}$$
$$- \mu\sigma^{200} + \Delta\sigma^{120} + m\sigma^{233},$$
$$d_1(\boldsymbol{k}) = t_1(\cos k_1 + \cos k_2 + 1),$$
$$d_2(\boldsymbol{k}) = t_1(\sin k_1 + \sin k_2),$$
$$d_3(\boldsymbol{k}) = 2t_2[\sin k_2 - \sin k_1 + \sin(k_1 - k_2)], \qquad (13)$$

where $k_1 = k_x$ and $k_2 = \frac{1}{2}k_x + \frac{\sqrt{3}}{2}k_y$. $\sigma^{abc} = \sigma^a \otimes \sigma^b \otimes \sigma^c$, the three Pauli spaces correspond to the (1) real and imaginary parts of the electron operator, (2) the valley space, and (3) the sublattice space of the effective Haldane model respectively.

The horizontal domain wall in Fig. 1(a) breaks the valley conservation, and hence will induce intervalley scattering between the edge states of the two valleys. This effect is modeled by an intervalley scattering $M\sigma^{211}$ on half of an open
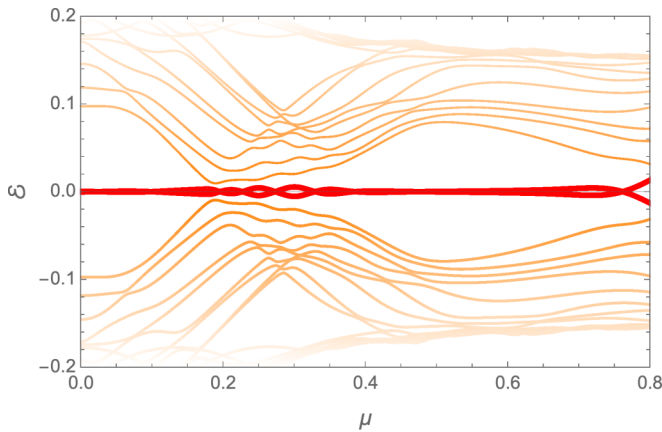
FIG. 3. The low-energy modes of our effective lattice model plotted against chemical potential, with $s$-wave valley-singlet pairing amplitude $\Delta = 0.2$ in the bulk, and intervalley scattering $M = 0.8$ on half of the boundary. We observe two MZMs on the two $0d$ junctions between $M$ and $\Delta$ at the boundary, for a broad range of finite chemical potential, even when the bulk has finite charge carrier density.

boundary [Fig. 1(b)]. We expect one MZM on each of the $0d$ junctions between $\Delta$ and $M$ on the $1d$ boundary. With zero chemical potential, the existence of the MZM can be straightforwardly inferred from the Jackiw-Rebbi solution [70]. In fact, since the bulk is always gapped, we can view the $1d$ segment with nonzero backscattering $M$ as a $1d$ Kitaev chain. At $\mu = 0$, this Kitaev chain is in its topological nontrivial phase based on the Jackiw-Rebbi solution, and there is a MZM at its end. The Kitaev chain can still be in the topological nontrivial phase even when the bulk has finite charge density, since the bulk is gapped due to superconductivity, hence the MZMs can still persist. Indeed, we observe two MZMs with a broad range of chemical potential even when the bulk band has nonzero charge density (Fig. 3). The spatial wave function of these MZMs are plotted in Fig. 4 with chemical potential $\mu = 0.5$ (when the bulk has finite charge density), pairing amplitude $\Delta = 0.2$, and intervalley scattering $M = 0.8$ in our effective model.

Here we stress that a single localized Majorana fermion zero mode is stable against any perturbation, regardless of
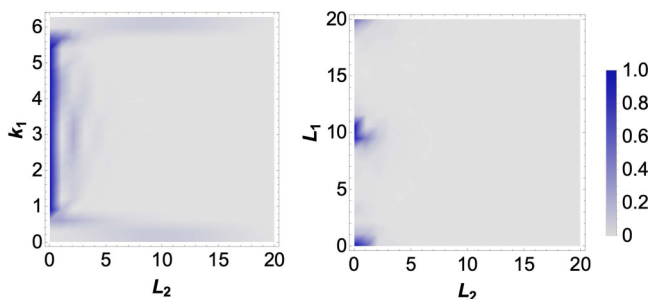


FIG. 4. (a) Penetration of the spatial wave function of the edge states (Fig. 2) into the bulk of Eq. (12), plotted against momentum $k_1$ along the boundary. (b) Spatial wave function of MZMs at the junctions between $\Delta$ and $M$ at the open boundary of our model [Fig. 1(b)], with chemical potential $\mu = 0.5$, $\Delta = 0.2$, and $M = 0.8$.

the symmetry of the system. This is why the classification of the Kitaev chain [71–73] without any symmetry is $\mathbb{Z}_2$, i.e., there is a nontrivial topological superconductor in $1d$ whose edge state is a single Majorana fermion zero mode which is stable against perturbations without assuming any symmetry. Multiple MZMs can be created by designing more corners of the domain wall in Fig. 1(a). Effective braiding of these MZMs can be achieved, and their non-Abelian statistics can be revealed by "measuring" these MZMs consecutively, without actually braiding them spatially [74,75].

## V. DISCUSSION

In this work we have discussed the interacting valley Chern insulator (VCI) that can be realized in moiré systems, and its classification under interaction. We demonstrate that although without interaction the classification of the VCI is $\mathbb{Z}$, interaction reduces the classification down to $\mathbb{Z}_3$, hence a VCI with valley Chern number 3 becomes a trivial insulator under interaction. This result implies that the VCI with valley Chern number 3 can be deformed continuously into a product state (atomic insulator) under interaction that preserves all the symmetries.

It is well known that a localized Wannier orbital cannot be constructed using single-particle states in a band with nontrivial band topology, which causes obstacles to using the standard tight-binding model and Hubbard model to describe the strong interaction effect when the topological band is doped with charge carriers. But since we demonstrated that VCI with valley Chern number 3 is trivialized by interaction, a simple formalism to study doped interacting VCI with valley Chern number 3 becomes possible. In particular, it may be possible to construct an "interacting local Wannier orbital" which is not a simple linear combination of single-particle operators, but a combination of fermionic composite operators. This observation, if successful, will simplify theoretical study of some of the moiré systems tremendously. We will leave this observation to future explorations.

The mapping of interacting VCI to a bSPT also has potentially interesting consequences. The phase transition between a VCI with valley Chern number 1 and a trivial insulator is described by two massless Dirac fermions, and the extra time-reversal symmetry $\mathcal{T}$ mentioned in the text will guarantee one direct transition. While the topological-to-trivial phase transition of a bSPT state is described by a $N_f = 2$ QED$_3$ with noncompact U(1) gauge field [76,77]. The topological equivalence between the interacting VCI and bSPT implies that the physics around that topological-to-trivial phase transition of the interacting VCI can have two very different descriptions that are based on different quantum field theories.

[1] G. Chen, L. Jiang, S. Wu, B. Lv, H. Li, K. Watanabe, T. Taniguchi, Z. Shi, Y. Zhang, and F. Wang, Nat. Phys. **15**, 237 (2019).

[2] Y. Cao, V. Fatemi, A. Demir, S. Fang, S. L. Tomarken, J. Y. Luo, J. D. Sanchez-Yamagishi, K. Watanabe, T. Taniguchi, E. Kaxiras *et al.*, Nature **556**, 80 (2018).

[3] Y. Cao, V. Fatemi, S. Fang, K. Watanabe, T. Taniguchi, E. Kaxiras, and P. Jarillo-Herrero, Nature **556**, 43 (2018).

[4] M. Yankowitz, S. Chen, H. Polshyn, Y. Zhang, K. Watanabe, T. Taniguchi, D. Graf, A. F. Young, and C. R. Dean, Science **363**, 1059 (2019).

[5] G. Chen, A. L. Sharpe, P. Gallagher, I. T. Rosen, E. Fox, L. Jiang, B. Lyu, H. Li, K. Watanabe, T. Taniguchi *et al.*, Nature **572**, 215 (2019).

[6] A. L. Sharpe, E. J. Fox, A. W. Barnard, J. Finney, K. Watanabe, T. Taniguchi, M. A. Kastner, and D. Goldhaber-Gordon, Science **365**, 605 (2019).

[7] P. Kim, Ferromagnetic superconductivity in twisted double bilayer graphene, http://online.kitp.ucsb.edu/online/bands_m19/kim/ (2019), Talks at KITP, Jan 15, 2019.

[8] X. Lu, P. Stepanov, W. Yang, M. Xie, M. A. Aamir, I. Das, C. Urgell, K. Watanabe, T. Taniguchi, G. Zhang *et al.*, arXiv:1903.06513.

[9] C. Shen, N. Li, S. Wang, Y. Zhao, J. Tang, J. Liu, J. Tian, Y. Chu, K. Watanabe, T. Taniguchi *et al.*, arXiv:1903.06952.

[10] X. Liu, Z. Hao, E. Khalaf, J. Y. Lee, K. Watanabe, T. Taniguchi, A. Vishwanath, and P. Kim, arXiv:1903.08130.

[11] Y. Cao, D. Rodan-Legrain, O. Rubies-Bigorda, J. M. Park, K. Watanabe, T. Taniguchi, and P. Jarillo-Herrero, arXiv:1903.08596.

[12] R. Bistritzer and A. H. MacDonald, Proc. Natl. Acad. Sci. **108**, 12233 (2011).

[13] E. Suárez Morell, J. D. Correa, P. Vargas, M. Pacheco, and Z. Barticevic, Phys. Rev. B **82**, 121407(R) (2010).

[14] S. Fang and E. Kaxiras, Phys. Rev. B **93**, 235153 (2016).

[15] G. Trambly de Laissardière, D. Mayou, and L. Magaud, Phys. Rev. B **86**, 125413 (2012).

[16] Y.-H. Zhang, D. Mao, Y. Cao, P. Jarillo-Herrero, and T. Senthil, Phys. Rev. B **99**, 075127 (2019).

[17] B. L. Chittari, G. Chen, Y. Zhang, F. Wang, and J. Jung, Phys. Rev. Lett. **122**, 016401 (2019).

[18] J. Y. Lee, E. Khalaf, S. Liu, X. Liu, Z. Hao, P. Kim, and A. Vishwanath, arXiv:1903.08130.

[19] J. Liu, Z. Ma, J. Gao, and X. Dai, Phys. Rev. X **9**, 031021 (2019).

[20] G. Chen, A. L. Sharpe, E. J. Fox, Y.-H. Zhang, S. Wang, L. Jiang, B. Lyu, H. Li, K. Watanabe, T. Taniguchi *et al.*, arXiv:1905.06535.

[21] N. Bultinck, S. Chatterjee, and M. P. Zaletel, arXiv:1901.08110.

[22] Y.-H. Zhang, D. Mao, and T. Senthil, arXiv:1901.08209.

[23] C. Xu and L. Balents, Phys. Rev. Lett. **121**, 087001 (2018).

[24] J. F. Dodaro, S. A. Kivelson, Y. Schattner, X. Q. Sun, and C. Wang, Phys. Rev. B **98**, 075154 (2018).

[25] X.-C. Wu, A. Keselman, C.-M. Jian, K. A. Pawlak, and C. Xu, Phys. Rev. B **100**, 024421 (2019).

[26] C. Schrade and L. Fu, Phys. Rev. B **100**, 035413 (2019).

[27] L. Fidkowski and A. Kitaev, Phys. Rev. B **81**, 134509 (2010).

[28] L. Fidkowski and A. Kitaev, Phys. Rev. B **83**, 075103 (2011).

[29] L. Fidkowski, X. Chen, and A. Vishwanath, Phys. Rev. X **3**, 041016 (2013).

[30] C. Wang and T. Senthil, Phys. Rev. B **89**, 195124 (2014).

[31] Y.-Z. You and C. Xu, Phys. Rev. B **90**, 245120 (2014).

[32] X.-L. Qi, New J. Phys. **15**, 065002 (2013).

[33] S. Ryu and S.-C. Zhang, Phys. Rev. B **85**, 245132 (2012).

[34] H. Yao and S. Ryu, Phys. Rev. B **88**, 064507 (2013).

[35] Z.-C. Gu and M. Levin, Phys. Rev. B **89**, 201113(R) (2014).

[36] X. G. Wen and A. Zee, Phys. Rev. B **46**, 2290 (1992).

[37] X. G. Wen, Phys. Rev. Lett. **64**, 2206 (1990).

[38] X.-G. WEN, Int. J. Mod. Phys. B **06**, 1711 (1992).

[39] F. D. M. Haldane, Phys. Rev. Lett. **74**, 2090 (1995).

[40] M. Levin, Phys. Rev. X **3**, 021009 (2013).

[41] S. Liu, A. Vishwanath, and E. Khalaf, Phys. Rev. X **9**, 031003 (2019).

[42] T. O. Wehling, E. Şaşıoğlu, C. Friedrich, A. I. Lichtenstein, M. I. Katsnelson, and S. Blügel, Phys. Rev. Lett. **106**, 236805 (2011).

[43] A. H. Castro Neto, F. Guinea, N. M. R. Peres, K. S. Novoselov, and A. K. Geim, Rev. Mod. Phys. **81**, 109 (2009).

[44] X. Chen, Z.-C. Gu, Z.-X. Liu, and X.-G. Wen, Phys. Rev. B **87**, 155114 (2013).

[45] X. Chen, Z.-C. Gu, Z.-X. Liu, and X.-G. Wen, Science **338**, 1604 (2012).

[46] Z. Bi, R. Zhang, Y.-Z. You, A. Young, L. Balents, C.-X. Liu, and C. Xu, Phys. Rev. Lett. **118**, 126801 (2017).

[47] Y.-Z. You, Z. Bi, D. Mao, and C. Xu, Phys. Rev. B **93**, 125101 (2016).

[48] Y.-Z. You, Z. Bi, A. Rasmussen, M. Cheng, and C. Xu, New J. Phys. **17**, 075010 (2015).

[49] H. Song, S.-J. Huang, L. Fu, and M. Hermele, Phys. Rev. X **7**, 011020 (2017).

[50] Y.-M. Lu and A. Vishwanath, Phys. Rev. B **86**, 125119 (2012).

[51] X. G. Wen, Phys. Rev. Lett. **66**, 802 (1991).

[52] G. Moore and N. Read, Nucl. Phys. B **360**, 362 (1991).

[53] N. Read and D. Green, Phys. Rev. B **61**, 10267 (2000).

[54] D. A. Ivanov, Phys. Rev. Lett. **86**, 268 (2001).

[55] L. Fu, Phys. Rev. Lett. **104**, 056402 (2010).

[56] R. M. Lutchyn, J. D. Sau, and S. Das Sarma, Phys. Rev. Lett. **105**, 077001 (2010).

[57] Y. Oreg, G. Refael, and F. von Oppen, Phys. Rev. Lett. **105**, 177002 (2010).

[58] S. Jeon, Y. Xie, J. Li, Z. Wang, B. A. Bernevig, and A. Yazdani, Science **358**, 772 (2017).

[59] S. Nadj-Perge, I. K. Drozdov, J. Li, H. Chen, S. Jeon, J. Seo, A. H. MacDonald, B. A. Bernevig, and A. Yazdani, Science **346**, 602 (2014).

[60] L. Fu and C. L. Kane, Phys. Rev. Lett. **100**, 096407 (2008).

[61] J.-P. Xu, M.-X. Wang, Z. L. Liu, J.-F. Ge, X. Yang, C. Liu, Z. A. Xu, D. Guan, C. L. Gao, D. Qian *et al.*, Phys. Rev. Lett. **114**, 017001 (2015).

[62] P. Hosur, P. Ghaemi, R. S. K. Mong, and A. Vishwanath, Phys. Rev. Lett. **107**, 097001 (2011).

[63] Z. Wang, P. Zhang, G. Xu, L. K. Zeng, H. Miao, X. Xu, T. Qian, H. Weng, P. Richard, A. V. Fedorov *et al.*, Phys. Rev. B **92**, 115119 (2015).

[64] G. Xu, B. Lian, P. Tang, X.-L. Qi, and S.-C. Zhang, Phys. Rev. Lett. **117**, 047001 (2016).

[65] K. Jiang, X. Dai, and Z. Wang, Phys. Rev. X **9**, 011033 (2019).

[66] X. Wu, S. Qin, Y. Liang, H. Fan, and J. Hu, Phys. Rev. B **93**, 115129 (2016).

[67] P. Zhang, K. Yaji, T. Hashimoto, Y. Ota, T. Kondo, K. Okazaki, Z. Wang, J. Wen, G. D. Gu, H. Ding *et al.*, Science **360**, 182 (2018).

[68] D. Wang, L. Kong, P. Fan, H. Chen, S. Zhu, W. Liu, L. Cao, Y. Sun, S. Du, J. Schneeloch *et al.*, Science **362**, 333 (2018).

[69] F. D. M. Haldane, Phys. Rev. Lett. **61**, 2015 (1988).

[70] R. Jackiw and C. Rebbi, Phys. Rev. D **13**, 3398 (1976).

[71] A. Kitaev, AIP Conf. Proc **1134**, 22 (2009).

[72] A. P. Schnyder, S. Ryu, A. Furusaki, and A. W. W. Ludwig, AIP Conf. Proc. **1134**, 10 (2009).

[73] S. Ryu, A. Schnyder, A. Furusaki, and A. Ludwig, New J. Phys. **12**, 065010 (2010).

[74] P. Bonderson, M. Freedman, and C. Nayak, Phys. Rev. Lett. **101**, 010501 (2008).

[75] P. Bonderson, M. Freedman, and C. Nayak, Ann. Phys. **324**, 787 (2009).

[76] C. Xu and Y.-Z. You, Phys. Rev. B **92**, 220416(R) (2015).

[77] C. Wang, A. Nahum, M. A. Metlitski, C. Xu, and T. Senthil, Phys. Rev. X **7**, 031051 (2017).